Applied Catalysis B: Environmental 199 (2016) 447–457

Contents lists available at ScienceDirect

Applied Catalysis B: Environmental

journal homepage: www.elsevier.com/locate/apcatb

Degradation of benzotriazole by a novel Fenton-like reaction with mesoporous Cu/MnO_2: Combination of adsorption and catalysis oxidation

Yuting Zhang [a], Cao Liu [b], Bingbing Xu [c,**], Fei Qi [a,*], Wei Chu [d]

[a] Beijing Key Lab for Source Control Technology of Water Pollution, College of Environmental Science and Engineering, Beijing Forestry University, Beijing 100083, People's Republic of China
[b] Beijing Water Science Technology Institute, Beijing, 100048, People's Republic of China
[c] State Key Laboratory of Environmental Criteria and Risk Assessment, Chinese Research Academy of Environmental Sciences, Beijing 100012, People's Republic of China
[d] Department of Civil and Environmental Engineering, The Hong Kong Polytechnic University, Hung Hom, Kowloon, Hong Kong

ARTICLE INFO

Article history:
Received 20 February 2016
Received in revised form 9 May 2016
Accepted 2 June 2016
Available online 23 June 2016

Keywords:
Benzotriazole
Fenton-like
Mesoporous Cu/MnO_2
Chemisorption

ABSTRACT

Degradation of benzotriazole (BZA) as an emerging contaminant by a novel Fenton-like reaction was investigated using a catalyst prepared by incorporating Cu into mesoporous MnO_2 (mesoporous Cu/MnO_2, MCM). Catalysts were synthesized with different Cu contents, and were characterized by N_2 adsorption–desorption, X-ray photoelectron spectroscopy, ultraviolet–visible (UV–vis) diffuse reflectance spectroscopy, and temperature-programmed reduction (TPR)-H_2. The MCM functioned via surface chemisorption and redox reaction that was confirmed by intermediates identification, XPS and TPR analysis, followed by a Fenton-like oxidation derived by surface Cu^+ and Mn^{3+}, to provide high degradation efficiency for BZA in solution. Fourier transform infrared (FT-IR) spectroscopy result also verified the surface adsorption and Fenton-like reaction. MCM exhibited much higher adsorption and catalytic activity in the Fenton reaction than pure MnO_2 or CuO. The effect of Cu content in MCM, catalyst dose, H_2O_2 dose, and solution pH were investigated. BZA degradation was high in deionized water (removal efficiency = 89%) and moderate in wastewater treatment plant effluent (removal efficiency = 56%) after 60-min reaction at an initial pH of 7.13, which could be developed by adjusting the dose of catalyst or H_2O_2. A possible mechanism for the reaction is proposed. This involves surface adsorption with copper and a redox reaction with Mn^{3+}, followed by a copper–manganese cycle-derived Fenton-like reaction.

1. Introduction

Benzotriazole (BZA), a well-known ultraviolet absorbent and light stabilizer in aqueous medium, has been widely used in plastics, photographic paper, automotive coatings, and sunscreen [1]. Industrial applications of BZA include as corrosion inhibitors for copper and silver, cooling and hydraulic fluids, antifreeze, and aircraft deicing fluid [2–4]. Through its widespread application, considerable amounts of BZA have been released into the aquatic environment in direct discharge of effluents from industrial plants [5] and from urban wastewater treatment plants (WWTPs) [6]. The presence of BZA in the aqueous environment is harmful to ecosystems and human health [7]. Recently, BZA has been listed as an emerging contaminant [2], and many studies have documented that the conventional microbiology-based WWTP techniques cannot entirely degrade this compound because of its persistence [8]. Therefore, it is necessary to develop an effective technique to remove or degrade BZA present in effluent.

Advanced oxidation processes (AOPs) can be used to rapidly degrade a wide range of refractory organic substances in drinking water and wastewater [9]. AOPs include ozonation [10], photocatalysis [11], and the Fenton process [12]. The classic Fenton oxidation showed some features [13], as nonselectivity oxidation derived by hydroxyl radical (•OH) generated from H_2O_2 with Fe(II) [14], fast reaction rate, low cost, and low toxicity of reagents used. However, the homogeneous Fenton process also showed some significant drawbacks, such as the additional amounts of Fe^{2+} increasing the

* Corresponding author at: P.O. 60, Beijing Forestry University, No. 35 Qinghua East Road, Haidian District, People's Republic of China.
** Corresponding author.
E-mail addresses: xbb_hit@126.com (B. Xu), qifei@bjfu.edu.cn, qifei_hit@163.com (F. Qi).

http://dx.doi.org/10.1016/j.apcatb.2016.06.003
0926-3373/

formation of ferric hydroxide sludge [15], and the narrow available range of solution pH values (2–4) [16]. In order to overcome these drawbacks, the heterogeneous Fenton-like reaction is considered as a more practical and efficient alternative technique [17]. In addition, many studies have investigated iron-free catalysts, such as copper [18,19], manganese [20], and cerium [21], for Fenton-like reactions to broaden the pH range and avoid sludge formation.

In order to extend on these studies, the aim of this study was to develop a catalyst based on copper and manganese oxides to improve the performance of the heterogeneous Fenton-like process for degradation of BZA in aqueous medium. The developed catalyst is referred to as mesoporous Cu/MnO_2 (MCM). The surface topography and chemical properties of the MCM were characterized in detail, and its performance for degradation of BZA in a Fenton-like reaction was evaluated in both distilled deionized water (DDW) and effluent from a WWTP. A reaction mechanism for the Fenton-like reaction was proposed based on the intermediates identification.

2. Materials and methods

2.1. Chemicals and reagents

All chemicals were of analytic reagent grade and all solvents were of high-performance liquid chromatography (HPLC) grade. All chemicals and solvents were used as received without further purification. Peroxide (98%) and BZA (99%) were purchased from Sigma-Aldrich Inc. (St. Louis, MO, USA). DDW with a resistivity of 18.2 MΩ cm was generated using a Barnstead Nanopure water treatment system (Thermo Fisher Scientific Inc., Waltham, MA, USA) and used to prepare all the solutions in this study. Nitric acid and/or sodium hydroxide were used to adjust the initial pH of each solution. For preparation of the catalyst under different conditions, $KMnO_4$, $CuSO_4{\cdot}5H_2O$, and maleic acid (Sigma-Aldrich Inc.) were used.

2.2. Synthesis and characterization of MCM

Solution A was prepared by dissolving potassium permanganate (30.0 mmol) and $CuSO_4{\cdot}5H_2O$ (7.5 mmol) in 50 mL of DDW. Solution B was prepared by dissolving maleic acid in DDW at 200 mmol L^{-1}, and this solution was used as a reductant. Freshly prepared solution B was added into freshly prepared solution A to reduce the potassium permanganate, and the mixture was stirred for 1 h. After aging for 24 h at room temperature to complete the redox reaction, a black or brown gel was obtained. This gel was washed with DDW until the conductivity of the supernatant was constant. After drying at 70 °C overnight, MCM was obtained by calcination in air at 300 °C for 2 h. Under typical synthetic conditions, the MCM showed a Cu/Mn molar ratio of 1:4. MCM prepared with different copper contents were labeled as x_{Cu}MCM (x_{Cu} is the amount-of-substance fraction of copper, e.g., 20.00% MCM). Mesoporous manganese (MM) oxide without copper was also prepared as above without addition of $CuSO_4{\cdot}5H_2O$ [22]. The methods used for characterization of MM and MCM are shown in Text S1 in the Supplementary Material.

2.3. Fenton-like reaction procedure

Adsorption or oxidation of BZA was carried out in a 200-mL glass reactor containing 100 mL of a 0.05-mmol L^{-1} BZA solution. The reactor was placed in a dark box at room temperature (24 °C). In the degradation experiments, the solutions were either premixed or not premixed. In the premixed experiments, the catalyst (1.0 g L^{-1}) was first added to the BZA solution and the solution was allowed to stand for 30 min for the adsorption to reach saturation. Then, a known amount of H_2O_2 (10.0 mmol L^{-1}) from a stock solution was added to the mixture to start the Fenton-like reaction. Before addition of the catalyst, the solution pH was adjusted using nitric acid and/or sodium hydroxide solution, when DDW was used as the matrix. When the effluent of WWTP was used as the background (water quality was shown in our previous paper [23]), only BZA was spiked into it and no pH adjustment was made. At predetermined intervals, 2.0-mL samples were withdrawn using a syringe filter that did not show any adsorption for the parent compound. The oxidation was immediately quenched using a $Na_2S_2O_3$ solution (1.0 mol L^{-1}). In the nonpremixed experiments, H_2O_2 and MCM were added to the BZA solution simultaneously. The effects of changing various reaction parameters were investigated. All experiments were conducted in triplicate, and the data shown are averages with error bars. For testing the role of leached ions on this Fenton-like reaction, the experimental procedure was changed. First, premixing was conducted to leach potential ions for 30 min under different water pH; after that, the suspension was filtrated to separate the catalyst; and then H_2O_2 was added to the solution to test the role of potential leached ions on the activation H_2O_2. If the BZA decay was observed after the addition of H_2O_2, it was concluded that some ions were leached from catalyst in the premixing process and played some role for activation of H_2O_2. The analysis method of BZA and its intermediates, H_2O_2, and leached metal ions are shown in Text S2 in detail.

3. Results and discussion

3.1. Characterization of MCM

The results of analyses of the surfaces of MCM and MM are shown in Table 1. MM had a larger specific surface area than MCM. The presence of copper in MCM decreased the surface area and increased the pore diameter compared with MM. The mesopore and micropore volumes showed that the mesoporous structure was uniform as defined by IUPAC. The pore size distributions and N_2 adsorption–desorption isotherms are shown in Figs. S1(A) and (B), respectively. The isotherms are classified as type IV, typical of mesoporous materials. The hysteresis loop of MCM is smaller than MM, suggesting that the formed copper oxide particles filled into some micropore of MM. Without copper, MM exhibited two pore size distributions (1.5–5.0 and 5.0–30.0 nm). With introduction of copper in MCM, most of the pores were in the 5.0–30.0 nm range, which indicated that the copper did not change the mesopore structure of MM but did fill in the 1.5–5.0 nm pores. In order to get further insight into the microstructure of samples, the high-resolution transmission electron microscope (HRTEM) images of MCM are shown in Figs 1 (A) and S2. The MCM particles showed a uniform plate morphology with the average particle size of approximately 3.0–5.0 nm in diameter and the plate-like structure represents the horizontal or gradient nanoparticles. This result was also identified in scanning electron microscope (SEM) image (Fig. 1(D) and (E)). The plate grew in very high density and was arranged in a layered structure. MCM are composed of MnO_2 and the d-spacing of 0.234 nm corresponds to the distance of the (100) planes (Fig. 1(A)); however, no crystal plane of copper oxide was observed in this HRTEM image. The HRTEM image together with the energy-dispersive X-ray (EDX) spectrum of C, O, Mn, and Cu elements confirmed the presence of copper (Figs 1 (B) and S2). The EDX results of different points of images showed that the presence of O, Mn, and Cu was uniform (Fig. 1(C)). The peak corresponding to carbon is also obtained in the spectra, because powder was dispersed on a carbon-coated copper grid.

Fig. S3 shows results of X-ray photoelectron spectroscopy (XPS) for MM and MCM. The MM results showed the presence of manganese and oxygen, while copper emerged in MCM samples with or without reaction. Fig. 2(A) showed peaks originating from Cu $2p_{3/2}$

Table 1
Specific surface area and pore volume of catalysts, variation in chemical composition of MM, MCM, and after adsorption or catalytic reaction from XPS analysis.

Catalyst	BET surface area ($m^2\ g^{-1}$)	Total pore volume ($mL\ g^{-1}$)	Micropore volume ($mL\ g^{-1}$)	Average pore Diameter (nm)	Cu^+/Cu^{2+}	Mn^{3+}/Mn^{4+}	O_{ads}/O_{lat}
MM	386.765	0.696	0.000	7.194	–	0.43	0.17
MCM	215.423	0.536	0.008	9.959	0.29	0.41	0.29
Recycled after adsorption	173.404	0.414	0.000	9.559	0.31	0.52	0.30
Recycled after Fenton-like reaction	190.402	0.441	0.000	9.26923	0.34	0.50	0.32

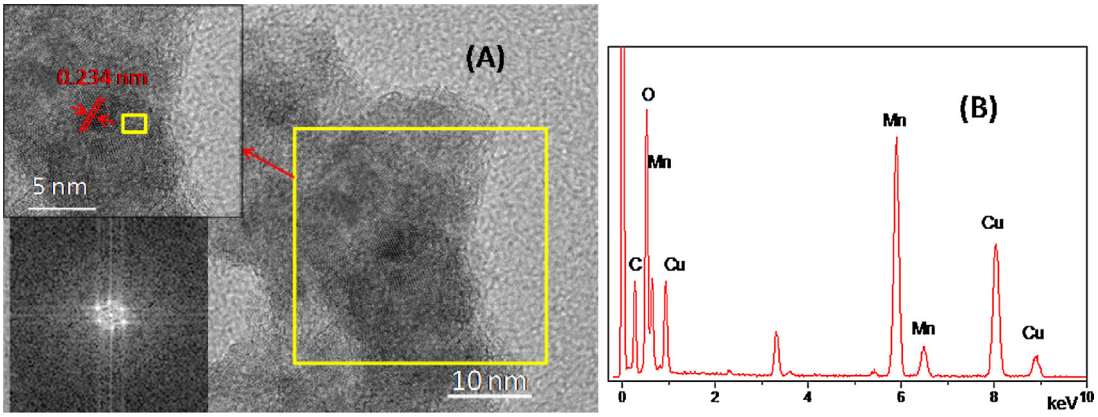

(C) EDX results of MCM

Elements	Wt.%	Wt.%	Wt.%	Average(%)	RSD(%)
C	6.65	14.13	11.73	10.84	25.74
O	24.23	23.08	25.87	24.39	4.03
Mn	36.55	30.52	34.94	34.00	6.83
Cu	32.57	32.27	27.46	30.77	3.59

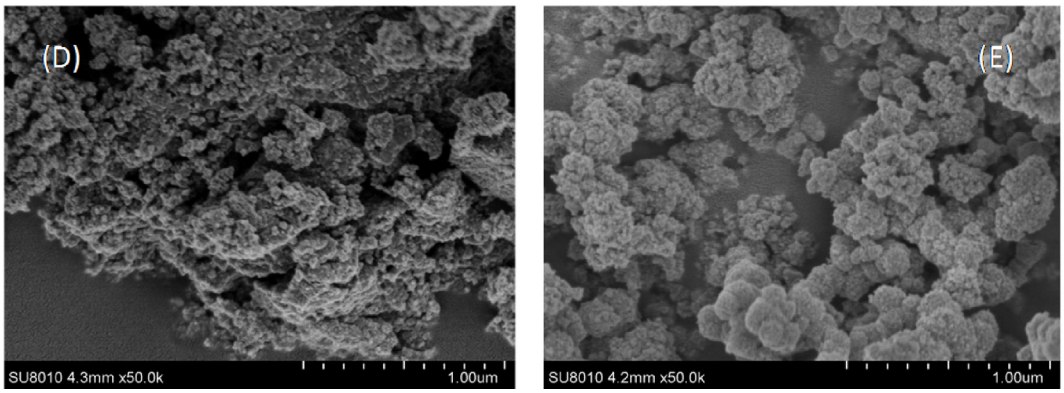

Fig. 1. (A) High-resolution transmission electron microscope (HRTEM) image of MCM; (B) The corresponding element analysis by EDX. (C) EDX results table of MCM. (D) SEM images of MM. (E) SEM images of MCM.

and Cu $2p_{1/2}$ at 932.3–934.3 and 952 eV [18,24,25] and satellite peaks. The presence of Cu^{2+} could be confirmed by the appearance of a peak at 934.3 eV and a shake-up satellite line at 940.0–945.0 eV. A peak at 932.8 eV was an evidence of the presence of a reduced copper species, which was also identified as Cu^+ based on the analysis of auger peaks of copper (Fig. S4). The ratio of Cu^+/Cu^{2+} was about 0.29:1 (Table 1) on the surface of MCM. The Mn 2p XPS spectrum exhibited two major peaks at 654.4 (Mn $2p_{1/2}$) and 642.6 eV (Mn $2p_{3/2}$) with a spin-energy separation of 11.8 eV (Fig. 2(B)) [26,27]. A peak at 641.8 eV was an evidence of the presence of Mn^{3+} species on the surface. The ratios of Mn^{3+}/Mn^{4+} were 0.43 and 0.41 on the surfaces of MM and MCM, respectively (Table 1). Therefore, the presence of copper did not change the ratio of the species of manganese present. Fig. 2(C) shows O 1s spectra, as peaks at 530 and 532 eV were assigned to lattice oxygen and surface hydroxyl groups, respectively [28,29]. MM showed a stronger lattice oxygen peak and weaker surface hydroxyl group peak than MCM, indicating that copper incorporation increased more oxygen defect leading more density of surface hydroxyl groups that was conventional reaction sites for surface adsorption [30] and catalytic oxidation [31]. Temperature-programmed reduction (TPR) was performed to investigate the oxidation–reduction properties of the samples (Fig. 2(D)). For MM, peaks located at 275 and 300 °C were attributed to the reduction of $Mn^{4+} \rightarrow Mn^{3+}$ and

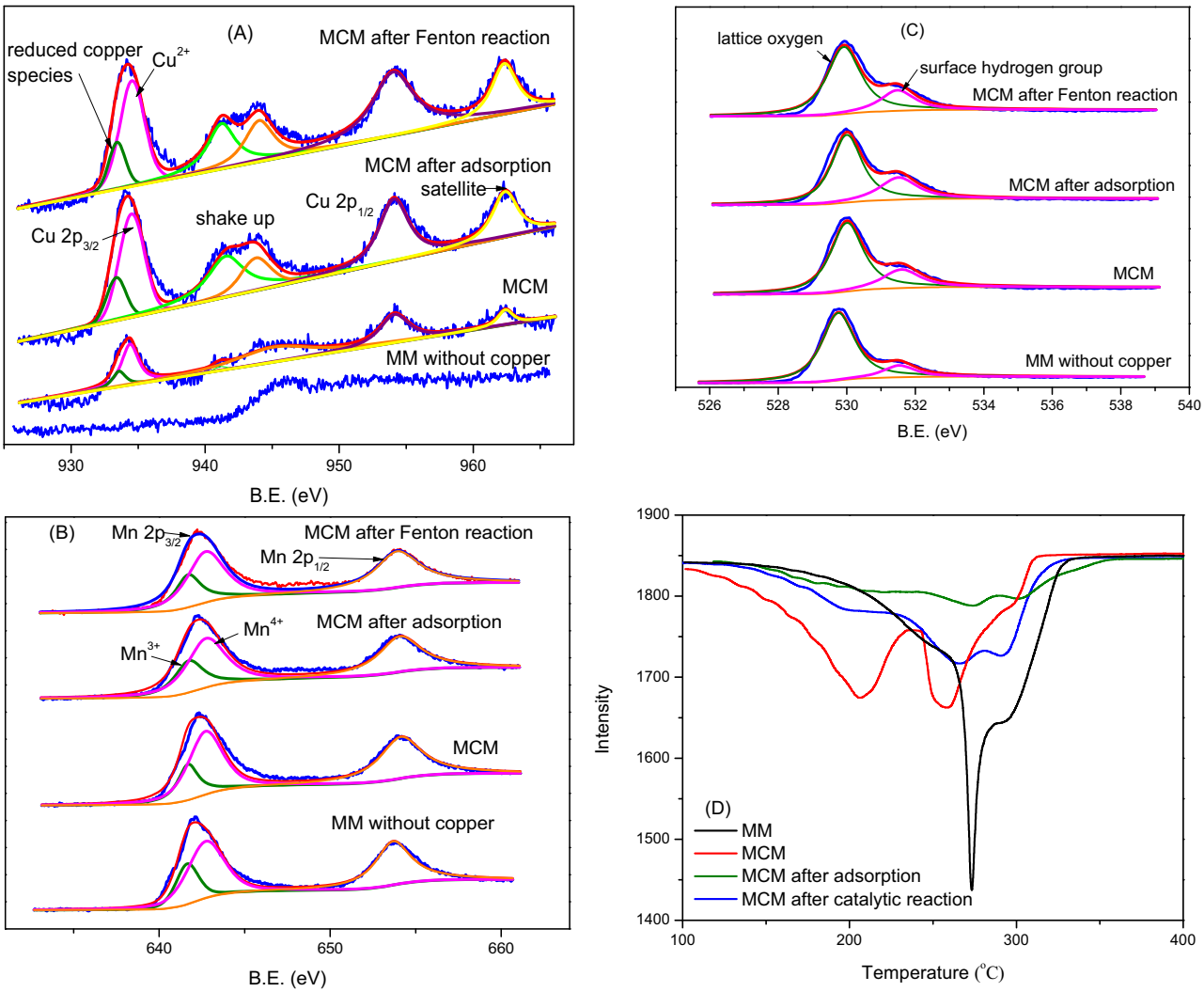

Fig. 2. XPS characterization of catalysts Cu (A), Mn (B), and O (C); TPR-H_2 characterization of catalyst (D).

$Mn^{3+} \rightarrow Mn^{2+}$, respectively [27,32]. After the introduction of copper to form MCM, hydrogen consumption peaks appeared at 170 and 208 °C, which were attributed to reduction of copper oxide species $Cu^{2+} \rightarrow Cu^{+}$ and $Cu^{+} \rightarrow Cu^{0}$, respectively [32]. The second hydrogen consumption exhibited peaks at 255 and 300 °C as the manganese reduction. The introduction of copper decreased the temperature of the manganese reduction, promoting mobility of lattice oxygen in MnO_2 and improving the reducibility of MnO_2. This would make the manganese component more reactive to the catalytic oxidation. In addition, the intensity of the reduction peak in MCM was lower than that in MM, indicating that oxidant components in the catalyst were reduced more easily and the catalyst was more reactive. The corresponding ultraviolet–visible (UV–vis) diffuse reflectance spectrums are presented in Fig. S5. The spectrum of MM showed peaks at 279 and 499 nm, which were characteristic of Mn^{3+} and Mn^{4+}, respectively [33]. After introducing copper to form MCM, new bands appeared in the 320- to 450-nm regions and were evidence of the presence of Cu^{2+} on the catalyst surface [34]. The intensity of the bands in the 455 to 485 nm regions was evidence of the presence of Cu^{+} ions. XPS, TPR, and UV–vis diffuse reflectance spectroscopy showed the same results for copper and manganese. In order to investigate surface functional group of MM and MCM, FT-IR spectra of the samples are presented in Fig. S6. The presence of peaks at 525 and 608 cm^{-1} of MM and MCM was related to the stretching vibrations of metal oxygen (Me-O) [35]. The appearance of two peaks at 3430 and 1633 cm^{-1} were mainly because of the bending vibration of the surface hydroxyls and absorbed water [36], respectively. MCM showed a stronger surface hydroxyls peak than MM, indicating that the incorporation of copper increased the oxygen defect, which was consistent with results of XPS and TPR and would show a significant effect on adsorption or Fenton oxidation.

3.2. *Performance of the Fenton-like reaction with MCM for degradation of BZA*

The Fenton-like reaction activity of the prepared catalyst was evaluated for degradation of BZA with H_2O_2. In the premixed experiments, a control test with MM showed negligible adsorption and degradation (Fig. 3(A)). Another control test with CuO as the catalyst resulted in the removal of almost 30% of the BZA after 3 h. With the MCM, both the adsorption and oxidation efficiencies of BZA increased with increasing Cu content in the catalyst. When the copper content was increased above 50%, the adsorption performance increased to the most capacity. The joint result was obtained when MCM was used, suggesting that the significant oxygen defect and surface hydroxyl group led by the incorporation of copper into MM oxide were the main contributors. Furthermore, the surface area of MCM was significantly decreased after the incorporation of copper, which is conflicted with the above results. Therefore, it was concluded that specific surface area was not the derived force for

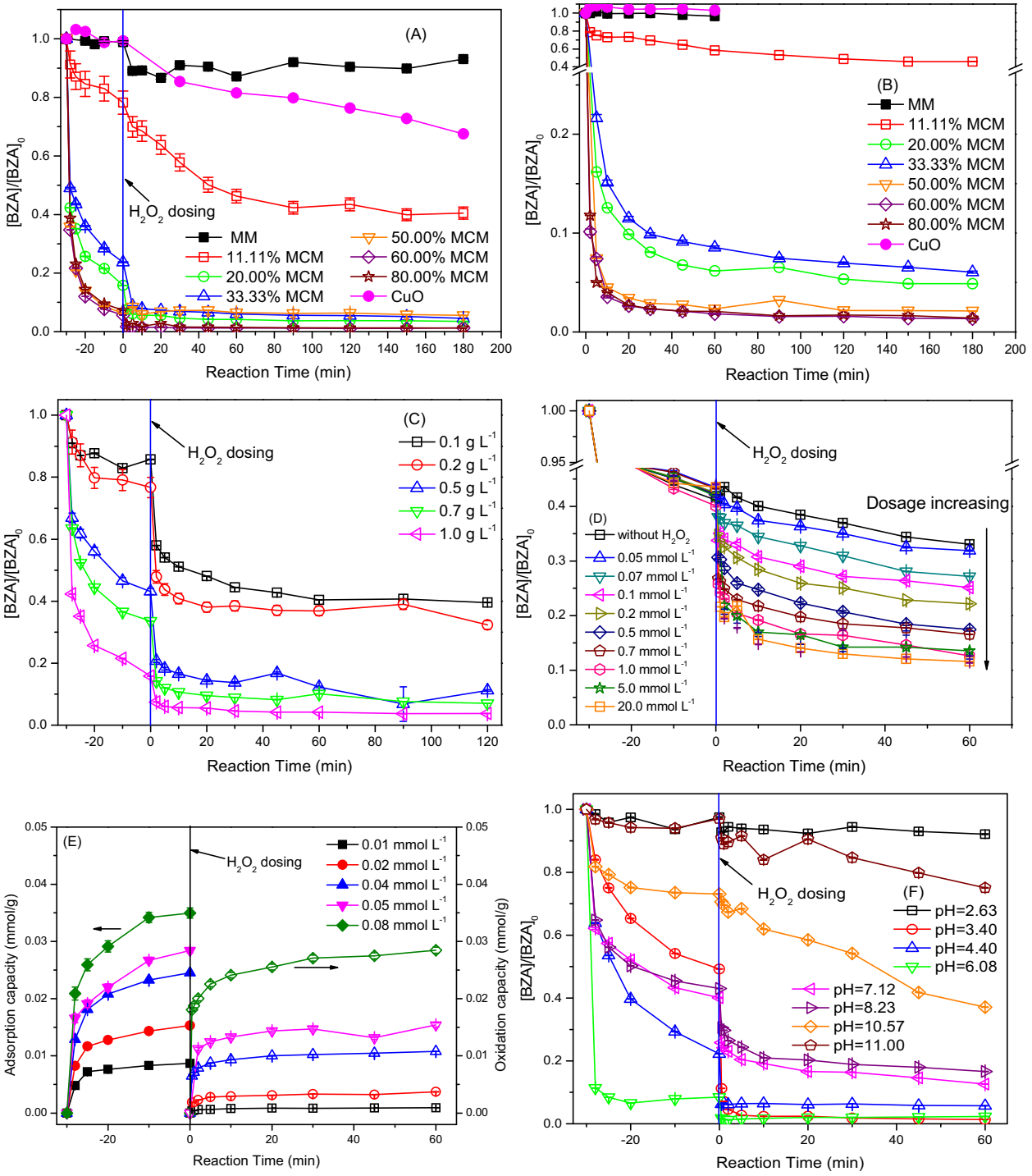

Fig. 3. Effect of Cu content in catalyst on the performance of BZA degradation in Fenton-like reaction with MCM, (A) in premixed mode; (B) in without premixed mode; (C) effect of MCM dose; (D) effect of H_2O_2 dose; (E) effect of initial concentration of BZA; (F) effect of water pH. Reaction condition: $[BZA]_0 = 0.05$ mmol L^{-1}, $[H_2O_2] = 10.0$ mmol L^{-1}, [MCM] = 1.0 g L^{-1}, water pH = 7.13 adjusted by HNO_3 and NaOH, in (C), (D), and (E) the corresponding parameters were changed in figures.

the surface adsorption and catalysis oxidation, but was derived by surface hydroxyl group. Compared with the FT-IR spectra (Fig. S6) of fresh MCM and MCM after the adsorption or Fenton reaction, it was showed that the peak intensity of surface hydroxyl group decreased, indicating that surface hydroxyl group took part in the reaction and played an important role in both adsorption and catalytic oxidation. More than 90% of the BZA was degraded in the premixed experiments after 180-min Fenton-like oxidation at neutral pH with catalysts containing 20.00–80.00% copper. The good performance of this reaction at neutral pH widens the pH range. The removal of BZA in the premixed experiments was the same as that in the nonpremixed experiments (Fig. 3(B)), indicating that preadsorption was not a key step for control of BZA degradation. When the amount of copper was >20%, similar performance was obtained in the premixed and nonpremixed experiments. In order to minimize the amount of copper used in the preparation and avoid potential leaching of copper from the catalyst, the 20% Cu catalyst was used in subsequent experiments.

The effect of the MCM dose on BZA degradation is shown in Fig. 3(C). When the dose of MCM increased, the adsorption of BZA

also increased. This trend was also observed in the Fenton-like reaction. When the MCM dose was increased from 0.2 to 0.5 g L^{-1}, there were significant increases in both the adsorption and oxidation. Fig. 3(D) shows the effect of altering the dose of H_2O_2 on the degradation of BZA with MCM. Overall, the removal of BZA increased as the H_2O_2 dose increased. This effect was negligible when the H_2O_2 dose was increased from 0.0 to 0.05 mmol L^{-1}, but was significant when the H_2O_2 dose was increased from 0.05 to 0.7 mmol L^{-1}. After this point, the development effect was slight, indicating that the reactive site provided by MCM was not enough to active H_2O_2. When H_2O_2 dose was 20.0 mmol L^{-1}, almost no performance development was observed in this study, confirming no active site was available to active overdose H_2O_2. The trend of effect of H_2O_2 dose was not consistent with that in other studies, as it first increased and then decreased [37], indicating that MCM prepared in this study supplied a strong capacity to active H_2O_2. The result of Fig. 3(D) shows that the optimum H_2O_2 dose (ratio of H_2O_2/BZA of 14:1) in this study was lower than that in other studies [38], which suggests that the MCM shows higher catalytic activity and usage rate of H_2O_2 than other catalysts. The effect of the initial concentration of BZA on the performance is shown in Fig. 3(E). Stronger adsorption and oxidation capacity were observed as the initial concentration of BZA increased. No negative effect was observed as the initial concentration of BZA ranged from 0.01 to 0.08 mmol L^{-1}, indicating that MCM showed higher adsorption and oxidation capacity, and a better performance on BZA degradation. The surface adsorption of MCM was higher than the Fenton-like reaction. Fig. 3(F) shows the effect of the initial pH of the solution on the performance in the premixed experiments. A narrow pH range is one of the major limitations of the application of homogeneous or iron-based heterogeneous Fenton reactions in water treatment [39]. However, the use of a copper or manganese catalyst in a Fenton-like reaction has been shown to widen the functional pH range [40]. In this study, better performance for BZA removal was observed with pH values between 3.40 and 8.23. MCM retained almost its high catalytic activity over a wide pH range, even under neutral conditions. The decrease of water pH during this reaction was very slight because of the formation of acidic intermediates (Fig. S7). As the initial concentration of BZA was not too high, the concentration of the generated acid intermediates would not be too high. Therefore, the solution pH variation is very slight. However, the adsorption capacity and catalytic activity were dependent on the initial solution pH, and this effect is discussed in detail in Section 3.5.

Reuse of MCM for the Fenton-like reaction was evaluated with five consecutive experiments (Fig. 4(A)). The used catalyst was isolated by filtration, washed with DDW thrice, and dried at 70 °C before reuse. The performance of MCM on BZA degradation via the Fenton-like reaction decreased as the number of reuse cycles increased. In the first three cycles, the removal efficiency of BZA decreased slightly. In the third cycle, almost 80% of the BZA was removed, and this was only about 10% lower than that in the first test. In the next two cycles, the removal of BZA decreased more, and this could be attributed to the following: (1) variation of the valence of copper and manganese, or leaching of copper and manganese from catalyst and (2) surface adsorption of intermediates generated from BZA, inhibiting the following Fenton-like reaction. The performance of the catalyst with effluent from a WWTP is shown in Fig. 4(B). The water quality of the effluent used in this study is discussed in a previous publication [23]. In this study, the concentration of BZA in the effluent of WWTP was not measured. According to a previous publication, the occurrence concentration of BZA in influent and effluent of WWTPs ranged from 0.131 to 44.0 μg L^{-1} and 0.2 to 18.0 μg L^{-1}, respectively [41–44]. In this study, 0.05 mmol L^{-1} (2.975 mg L^{-1}) BZA was spiked into the effluent of WWTP. This concentration was much higher than the reported occurrence concentration. Therefore, if a good degradation performance was observed in this novel Fenton-like reaction, better removal efficiency would be observed in WWTP, because the occurrence concentration of BZA in WWTP was much lower than the simulated one. Compared with BZA removal from DDW (removal efficiency = 89%), the removal efficiency from WWTP effluent was lower (56%) after 60 min with an initial solution pH of 7.13. However, the performance for BZA degradation in the effluent was improved when the dose of the catalyst or H_2O_2 was increased. The effect of increasing the H_2O_2 dose on BZA degradation was more positive than that of increasing the catalyst dose. When the concentration in wastewater was >0.05 mmol L^{-1}, the removal efficiency would decrease, but would be increased by increasing the catalyst or H_2O_2 dose.

3.3. Role of homogeneous and heterogeneous Fenton reactions in BZA degradation

In MCM Fenton-like reaction, if the copper or manganese leached, the homogeneous Fenton-like reaction would contribute to the BZA decay and affect the safety of the effluent. Therefore, in this study, the roles of homogeneous and heterogeneous Fenton-like reactions in BZA degradation were studied here. First, MCM was added to the BZA solution for 30 min to release copper and/or manganese ion, and then the catalyst was separated from the solution. After this, H_2O_2 was added to the filtrate to start the oxidation (Fig. 4(C)). If copper and/or manganese ions were leached from the MCM, a homogeneous Fenton-like reaction would occur and lead to the decay of BZA. The effect of pH on ions leaching and its role in oxidation were investigated by altering the pH of the initial solution. Results showed that the degradation efficiency of BZA by Fenton-like reaction was about 10%, after releasing of ions with an initial solution pH of 3.40, indicating that the performance derived by the leaching ions was lower than the catalyst under acidic solution. Thus, it can be seen that copper and/or manganese ions were released under acidic conditions, but the concentration might be very low. The leached ions showed catalytic activity as the homogenous Fenton-like reaction, but only resulted in a small increase in the degradation efficiency. At an alkaline pH (10.57), the leached ions led to about 25% BZA degradation and the decreasing rate was higher than that in catalytic oxidation. This might be due to the higher efficient mass transfer in homogeneous reaction than heterogeneous one and the concentration of leached ions was higher than that in acidic solution. In general, drinking water or wastewater typically shows a neutral pH, and a neutral pH did not significantly affect the degradation of BZA in this study. This indicates that the concentration of leached ions was too low under neutral pH (the measured data were shown in Fig. S8) and showed less catalytic activity and slight homogeneous contribution for BZA decay. The leached manganese and copper ions were only 0.198 and 0.077 mg L^{-1} after Fenton-like reaction, respectively, which only correspond to 0.1165% and 0.05% of the MCM dose. When the MCM dose increased to 1.0 g L^{-1}, rapid BZA adsorption and oxidation were observed. However, leached concentration of metal ions was still low and almost no BZA degradation occurred under neutral pH. The effect of leached ions on the decomposition of H_2O_2 is shown in Fig. 4(D). At neutral pH, the leaching ions increased the decay of H_2O_2, but the decomposition was insufficient for BZA degradation (Fig. 4(C)). Therefore, MCM widened the water pH range for Fenton-like reaction that was dominated by heterogeneous reaction. Interestingly, the decay of H_2O_2 was enhanced after BZA adsorption on the surface of MCM (Fig. 4(D)). In many other studies, adsorption of the parent compound on the surface of catalyst has negatively affected decay of H_2O_2 [45,46]. The enhancement observed in this study could be a key factor behind the better degradation of BZA obtained with MCM compared with other catalysts, and this will be discussed in detail in Section 3.5.

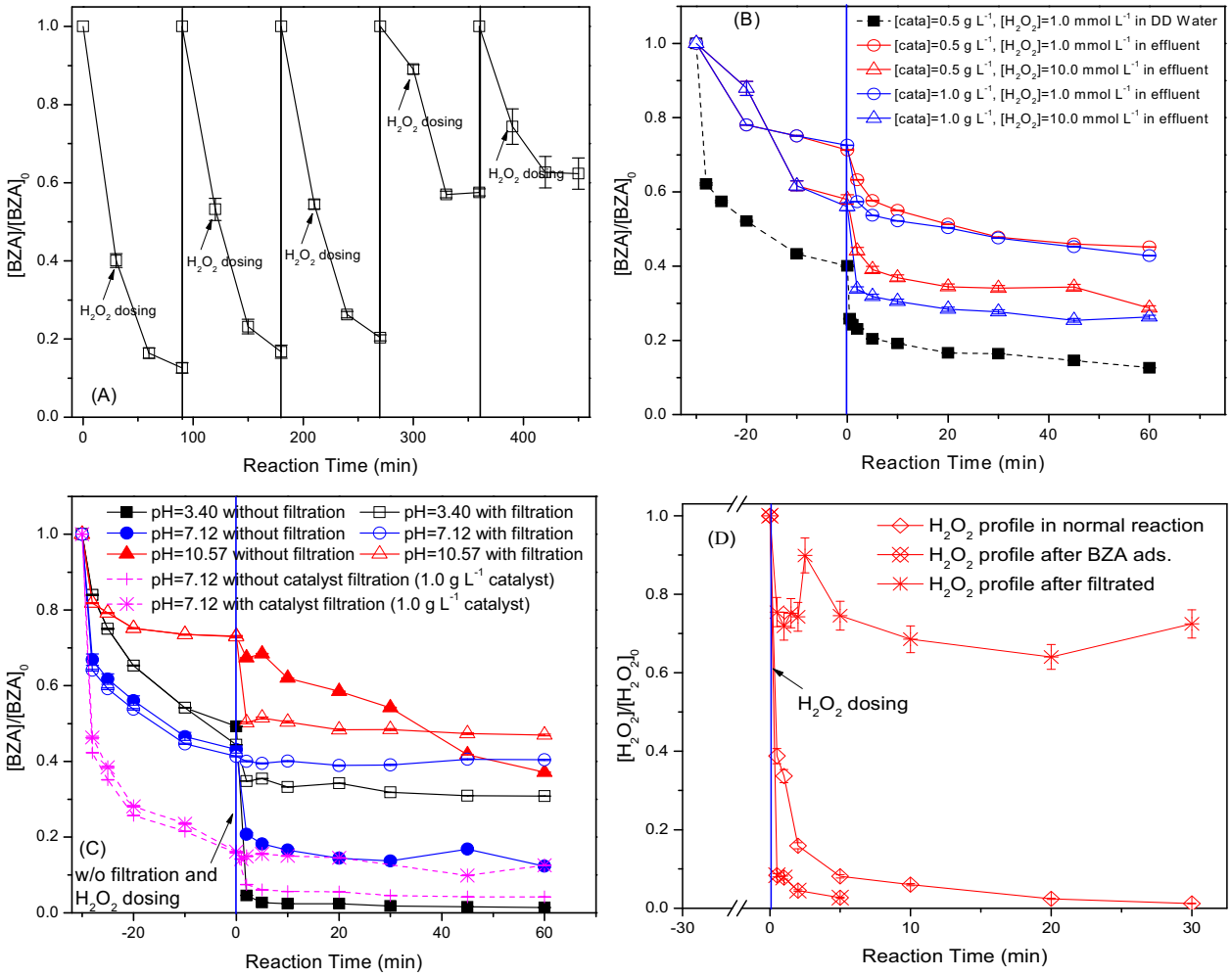

Fig. 4. (A) Effect of reuse/recycle; (B) effect of effluent of WWTP; (C) role of leached ions in the catalytic oxidation; (D) role of leached ions on H_2O_2 decomposition. Reaction condition: (A) $[BZA]_0 = 0.05$ mmol L^{-1}, $[H_2O_2]_0 = 1.0$ mmol L^{-1}, $[MCM]_0 = 0.5$ g L^{-1}, water pH = 7.13 adjusted by HNO_3 and NaOH; (B) $[BZA]_0 = 0.05$ mmol L^{-1} without adjusting the solution pH (7.16 ± 0.02); (C) and (D) $[BZA]_0 = 0.05$ mmol L^{-1}, $[H_2O_2]_0 = 1.0$ mmol L^{-1}, $[MCM]_0 = 0.5$ g L^{-1} for no specification, solution pH was adjusted by NaOH or HNO_3. The MCM catalyst was filtrated after 30-min adsorption to test the performance of the leached ions.

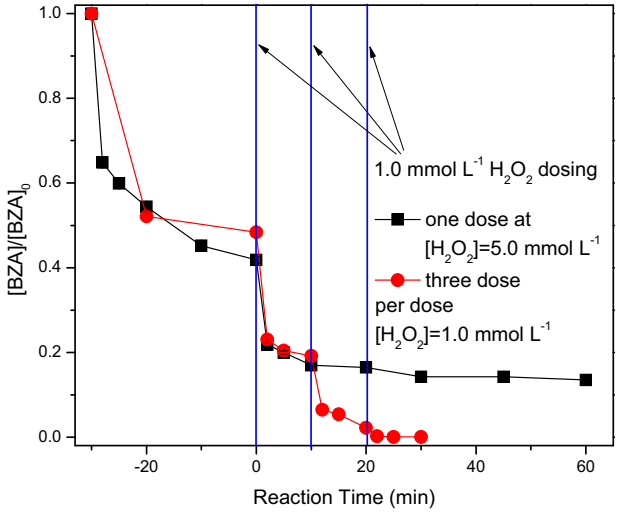

Fig. 5. H_2O_2 addition modes on the performance Reaction condition: $[BZA]_0 = 0.05$ mmol L^{-1}, $[MCM]_0 = 0.5$ g L^{-1}, water pH = 7.13 adjusted by HNO_3 and NaOH.

Fig. 5 shows the effect of different methods of H_2O_2 addition (e.g., all at once or in multiple aliquots) on BZA degradation. The BZA was almost completely removed within 30 min with a H_2O_2 concentration of 3.0 mmol L^{-1} achieved by addition of H_2O_2 to the reaction in three aliquots of 1.0 mmol L^{-1}. This performance was better than that obtained with one addition of 5.0 mmol L^{-1} H_2O_2. The incomplete BZA degradation in this case may result from a competitive reaction, in which excess H_2O_2 may react with reactive oxygen species (ROS) generated from the Fenton-like reaction, resulting in loss of oxidation ability. MCM showed excellent activity for H_2O_2 decomposition to generate ROS, and these might be scavenged by excess H_2O_2. These results show that after complete consumption of one H_2O_2 dose, another dose should be added to achieve better performance. In addition, a low H_2O_2 dose or multiple low-concentration aliquots should be used to reduce the cost of the MCM reaction.

3.4. *Effect of a radical scavenger on the degradation of BZA*

tert-Butyl alcohol (TBA) [47] or iodide (I^-) [48] can scavenge any •OH formed in solution or surface bound. In this study, neither TBA nor I^- affected degradation of BZA, indicating that •OH was not the dominated ROS in the solution or bound on the surface of catalyst in this Fenton-like reaction (Fig. 6(A)). This differs from the conventional homogeneous Fenton reaction and heterogeneous Fenton-like reaction using copper [31]. In order to confirm this

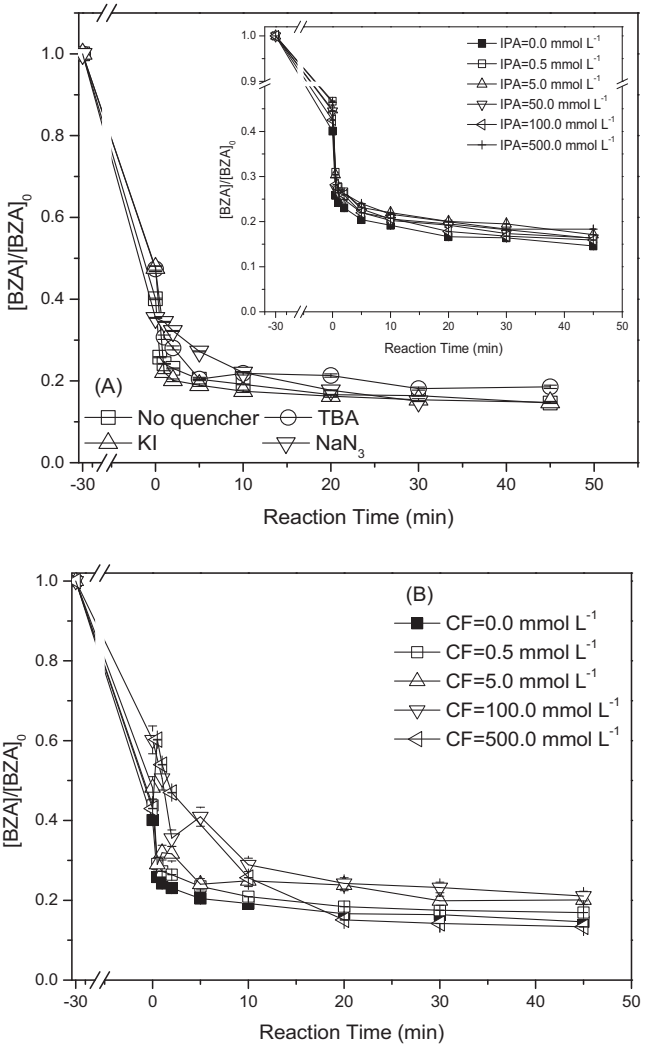

Fig. 6. Effect of radical quencher on the performance Reaction condition: $[BZA]_0 = 0.05\ mmol\ L^{-1}$, $[H_2O_2]_0 = 1.0\ mmol\ L^{-1}$, $[MCM]_0 = 0.5\ g\ L^{-1}$, [quencher] = 50.0 mmol L^{-1} without shown in figure, water pH = 7.13 adjusted by HNO_3 and NaOH.

result, a series of isopropanol (IPA) solutions (0.5–500 mmol L^{-1}; $k_{IPA,OH} = 1.9 \times 10^9\ M^{-1}\ s^{-1}$) [49] were used as another scavenger of •OH. Again, no influence on BZA degradation was observed (inset in Fig. 6(A)). Sodium azide (NaN_3), which is frequently used for scavenging singlet oxygen [47], also did not quench the reaction. Chloroform (CF) was used an $O_2^{\bullet-}$ scavenger ($k_{CF,O2^{\bullet-}} = 3 \times 10^{10}\ M^{-1}\ s^{-1}$) [50] in this study (Fig. 6(B)). The octanol–water portion coefficient of CF (1.97) indicates that it is not miscible with water. Therefore, CF would cover the surface of the catalyst and react with surface-bound $O_2^{\bullet-}$. The degradation of BZA decreased by about 4% in the presence of CF at 0.5 mmol L^{-1} and only 10% when the CF concentration was increased to 5.0 mmol L^{-1}. This inhibition was more remarkable when the CF concentration was increased to 500.0 mmol L^{-1}, at which the presence of CF might cover the surface of catalyst, indicating that $O_2^{\bullet-}$ was the important ROS in this reaction and was bound to the surface of the catalyst.

3.5. Surface adsorption and Fenton-like reaction mechanism

Heterogeneous Fenton-like reaction is combined by the surface adsorption and catalytic oxidation. The surface adsorption supplies a basic reaction platform for the sequence catalytic oxidation. The adsorption capacity, adsorption type (physical, chemical, or surface diffusion adsorption) from the isotherms [51], and kinetics studies [52] could explain the adsorption behaviors and mechanism, which were much useful to identify the role of the surface adsorption on the Fenton-like reaction. Therefore, the adsorption isotherm and kinetics were discussed here. The results of isothermal experiments to investigate the adsorption are shown in Fig. S9 and the parameters of isothermal models are shown in Table S1. All three isothermal models provided a good fit for the adsorption data, and the best among them was the Temkin model, indicating that the surface adsorption occurred via the chemisorption. Kinetics analysis of the adsorption is shown in Fig. S10 and the relevant parameters are shown in Table S1. Both a pseudo-second-order model and the Elovich model fit the experimental data well, which confirmed that the surface adsorption was dominated by chemisorption. BZA is a corrosion inhibitor for copper, and it has been reported that the nitrogen atoms in BZA donate electrons to Cu^+ to form a Cu^+–BZA [53] or Cu^{2+}–BZA complex [54], with the formation rate of the latter being much lower than that of the former [55]. Therefore, BZA could first bind with the Cu^+ of MCM, and then form the Cu^{2+}–BZA complex. This would decrease the concentration of copper at the surface and lead to reduction of the copper peak in Fig. 2(D). This was an important evidence for the chemisorption between BZA and MCM. XPS analysis of MCM was conducted after the surface adsorption (Fig. 2(B)), showing that the intensity of Mn^{3+} increased and that of Mn^{4+} decreased after surface adsorption (Table 1), suggesting that a surface redox reaction between BZA and MCM led to partial reduction of Mn^{4+} to Mn^{3+}. The oxidation of organic pollutants by MnO_2 has been reported previously [56,57]. Furthermore, three intermediates (B-1, B-2, and B-4) of the oxidation of BZA by Mn^{4+} were identified by liquid chromatography–mass spectrometry (LC–MS/MS) in the preadsorption phase (Table S2 and Fig. S13). It was considered that two reaction pathways occurred. The first being a two-step reaction at the organic compound–MnO_2 interface, involving surface complex formation and electron transfer [58]. Atom N8 of BZA with abundant charge and no steric hindrance was identified as active site [59]. A triazole ring-opening reaction at the N8 position would lead to generation of the intermediate. Oxidation with Mn^{4+} would release N8 from the triazole ring. At the same time, the remaining two nitrogen atoms will be converted to amino and nitro groups to generate intermediate B-1. Then, the transformation from the amino group to a nitro group will produce intermediate B-2. The second reaction pathway for the surface chemisorption involves oxidation of the parent compound by Mn^{4+}, leading to the formation of $C_6H_5N_3O$. Electrophilic substitutions will occur preferentially at the C2 positions, resulting in the formation of OH-BZA (B-4). Furthermore, both the intensity of Cu^{2+} and Mn^{4+} reduction decreased after the surface adsorption, indicating that BZA removal in the adsorption stage occurred via both adsorption to copper and oxidation by manganese. In addition, FT-IR spectra (Fig. S6) showed that the bands at 1570 and 1453 cm^{-1} appeared after the surface adsorption. The presence of 1570 and 1453 cm^{-1} was due to the bond of C=C stretching of the aromatic ring carbons [60]. This was important evidence for the BZA adsorption on the surface of MCM. This two-step surface reaction also resulted in the decrease of the pore volume in Fig. S1. The formed Mn^{3+} is an important species for H_2O_2 activation, leading to the increase of H_2O_2 activation after the preadsorption, which explained the result of the development of H_2O_2 decomposition after surface adsorption of BZA.

The adsorption capacity of BZA on MCM, being depended on the copper content, increased quickly to the platform as copper content increased from 0% to 20% (Fig. 7(A)). By contrast, when CuO was used as the catalyst, the adsorption capacity was close to zero. Therefore, the combination of mesoporous MnO_2 with copper oxide promotes surface adsorption of BZA derived by the formation of oxygen defect, and the absence of either one of these would

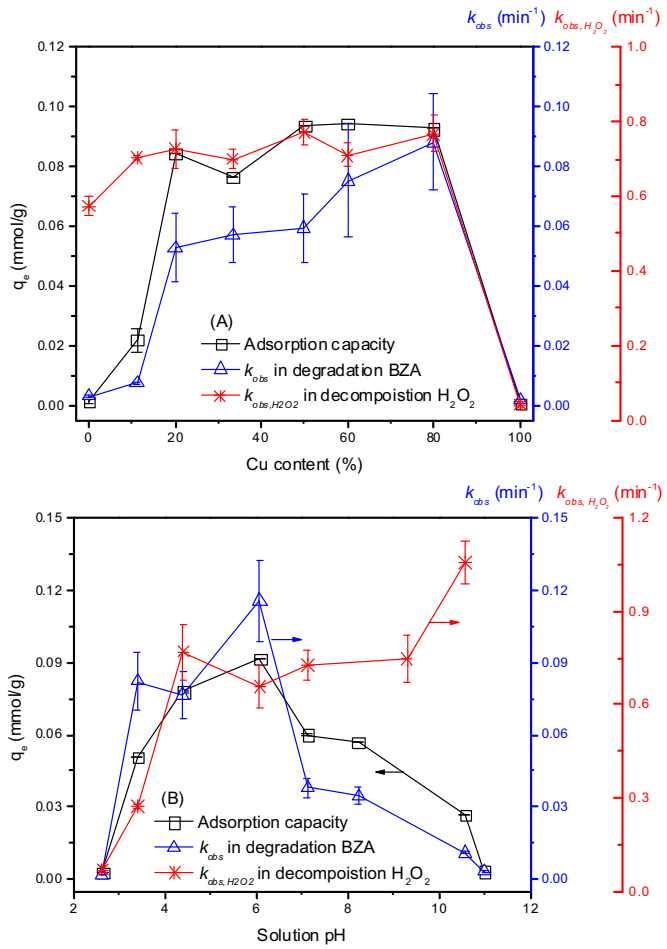

Fig. 7. Role of adsorption or radical oxidation in Fenton-like reaction with MCM. Reaction condition: $[BZA]_0 = 0.05$ mmol L^{-1}, $[H_2O_2]_0 = 1.0$ mmol L^{-1}, $[MCM]_0 = 0.5$ g L^{-1}, water pH = 7.13 adjusted by HNO_3 and NaOH.

stop surface adsorption. The solution pH influenced the adsorption capacity for two reasons (Fig. 7(B)). First, the solution pH changed the pattern of BZA and the charge of MCM. BZA has two pK_a, at 1.6 and 8.6 [61]. The pH values at the point of zero charge for MnO_2 and CuO are 4.5 and 9.2, respectively [62–64]. Therefore, the pH at the point of zero charge for MCM will fall in the range of 4.5–9.2, and should be closer to 4.5, because the amount of copper is only 20%. Therefore, at pH values between 4.5 and 7.12, the surface of MCM will show zero net charge and adsorb BZA through its surface hydroxyl groups via hydrogen bonding. This would increase sequence surface ligand copper and BZA and promote the redox reaction between BZA and Mn^{4+}. Under strongly acidic or alkaline conditions, there was electrostatic repulsion between MCM and BZA^+/BZA^-, which decreased the adsorption of BZA. In addition, manganese and/or copper ions will be leached from MCM to form the manganese hydroxide and copper hydroxide precipitates under alkaline conditions, which would disrupt the mesoporous structure of MCM and negatively affect the adsorption capacity.

The kinetic constant for the Fenton-like reaction was dependent on the copper content (Fig. 7(A)) and solution pH (Fig. 7(B)). The presence of copper improved the catalytic activity, and the absence of any metal components would stop the Fenton-like reaction. The H_2O_2 decomposition rate was dependent on the copper content and showed a similar trend for the kinetic constant for the Fenton-like reaction (Fig. 7(A)), indicating that most BZA degradation occurred with ROS that were formed from H_2O_2 decomposition. The presence of copper, which combined with mesoporous MnO_2, was a critical step for peroxide activation and BZA oxidation. Comparison of the XPS spectra of fresh MCM and MCM after the catalytic reaction showed that the intensity ratio of Cu^+/Cu^{2+} or Mn^{3+}/Mn^{4+} increased after the Fenton-like reaction (Table 1). This indicated that the Fenton-like reaction was promoted by cyclic reactions of copper and manganese. This result is consistent with that from the TPR curve. The H_2O_2 decomposition rate increased sharply when the pH was increased from 2.63 to 4.40, reached the platform, and increased again when solution pH increased over 9.3. Increase of the decomposition rate at solution pH > 6.08 did not contribute to the degradation of BZA, which could be attributed to the decreased surface adsorption capacity of BZA at these pH values. This result supported that the role of surface adsorption of BZA on MCM was critical.

As discussed above, a reaction mechanism for BZA degradation with MCM can be proposed, and this is shown in Scheme 1. In the first step, BZA is first adsorbed on the surface of MCM by surface hydroxyl group and Cu^{2+} or Cu^+. Then, surface oxidation of BZA occurs with Mn^{4+}, and this generates Mn^{3+}. In the second step, H_2O_2 decomposes via two pathways. The first of these is self-decomposition to form a proton and HO_2^- that continues to form an electron and $HO_2^{\bullet}$, which generates superoxide radical as the dominant ROS to degrade BZA. This process could be enhanced by the circular reaction between Mn^{3+} and Mn^{4+} [65,66]. The second H_2O_2 decomposition is catalytic decomposition by Cu^{2+} to generate Cu^+ and $HO_2^{\bullet}$, which then forms the superoxide radical [46]. In the third step, because of the standard potentials $\phi^{\theta}_{Cu^{2+}/Cu^{+}} = 0.159$ and $\phi^{\theta}_{Mn^{4+}/Mn^{3+}} = 0.95$, oxidation from Cu^+ to Cu^{2+} by Mn^{4+} occurred on the surface of MCM to complete the circulation reaction of copper. Then, decomposition of H_2O_2 began again. The transformation of the chemical structure of BZA in the Fenton-like reaction was also confirmed by LC–MS/MS (Table S2 and Fig. S13). In the Fenton-like stage, the oxidation continued because of surface adsorption and oxidation. An AOP occurred to form $(OH)_3$–BZA from B-4 through repeat hydroxyl substitution on the benzene ring. Benzene ring opening would occur at the C2 position to form carbonyl and hydroxyl through the advanced oxidation of OH-BZA or $(OH)_3$-BZA (B-7) by radicals generated from the Fenton-like reaction. From this intermediate, triazole ring opening at the N8 position caused by radicals led to the formation of two amino groups and a carbonyl group (intermediate B-6). B-8 was generated from the transformation of an amino group to a nitro group. After Fenton-like reaction, the peak of FT-IR (Fig. S6) appearing at 1740 cm^{-1} was due to the formation of C=O in carbonyl [36] that suggested the presence of B-6, B-7, and B-8. The peak at 1309 cm^{-1} was classified to the evidence of C—N bond that was in accordance with B-3 and B-7. In Fig. 8, the degradation of BZA via this Fenton-like reaction pathway is shown in black and the degradation pathway of BZA by surface Mn^{4+} is shown in red. Hence, in the overall oxidation process of BZA, the adsorption and oxidation complemented one another and increased the total degradation efficiency.

4. Conclusion

The adsorption and degradation of BZA by the developed MCM catalyst were dependent on the copper content. The MCM supported an adsorption or Fenton-like reaction platform. MCM showed higher catalytic activity in distilled water and effluent of WWTP, even at neutral pH. The superoxide radical was the important reactive oxide species in this reaction, and was bound to the surface of the catalyst. This was different from the conventional Fenton-like reaction involving copper. In the present Fenton-like reaction, the surface ligand of BZA with copper of MCM facilitated surface oxidation with Mn^{4+}, and the Fenton-like reaction was promoted by catalytic H_2O_2 decomposition and circular reac-

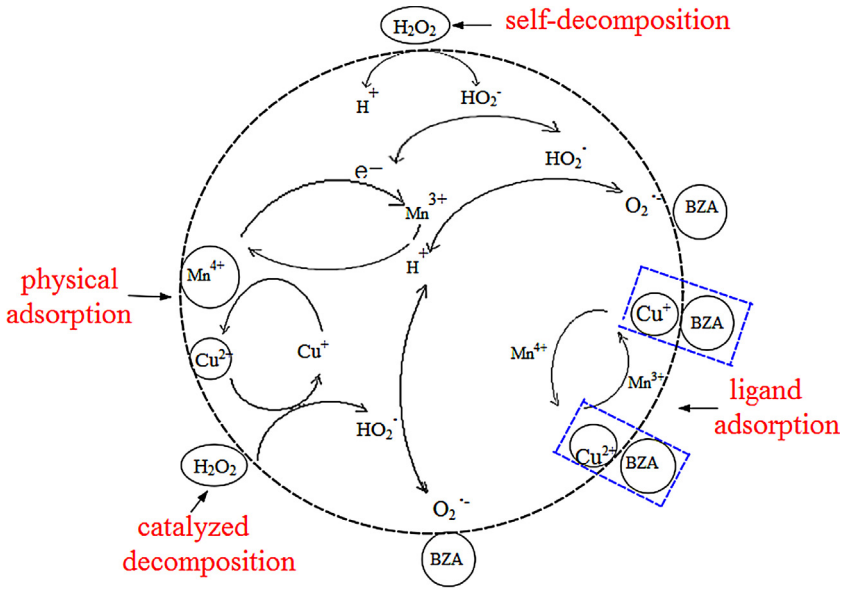

Scheme 1. Reaction mechanism of MCM Fenton-like reaction.

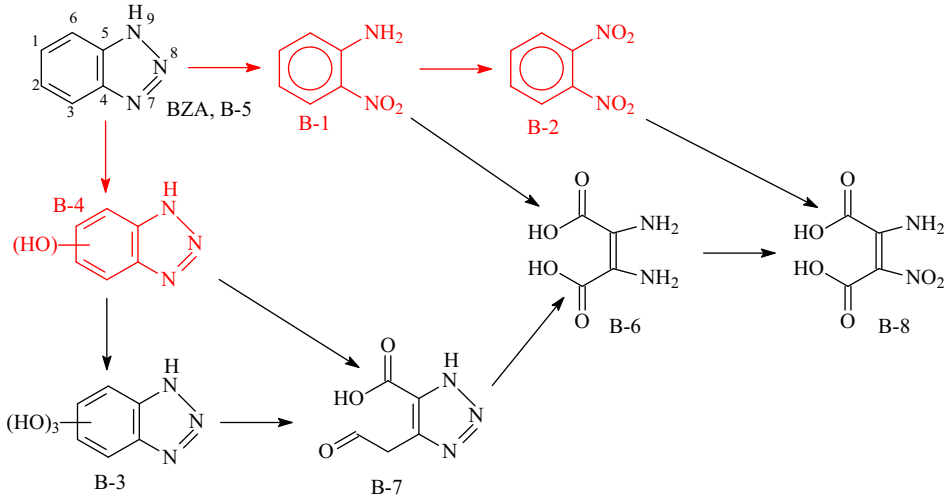

Fig. 8. Proposed transformation pathway of BZA by Fenton-like reaction derived by MCM.

tions between Mn^{4+}/Mn^{3+} and Cu^{2+}/Cu^{+}. A total of eight types of intermediates were generated and the fate of BZA was established for both the surface redox by Mn^{4+} and the Fenton-like reaction.

Acknowledgments

This study was carried out with the support of the Fundamental Research Funds for the Central Universities (No. 2016ZCQ03), the National Natural Science Foundation of China (No. 51578520, 51378063, 51108030, and 41273137), Beijing Natural Science Foundation (No. 8132033), and Beijing Science and Technology Projects (No. Z151100002115008). Sincere thanks go to the peer reviewers and editor for providing valuable comments to improve the quality of this manuscript.

Appendix A. Supplementary data

Supplementary data associated with this article can be found, in the online version, at http://dx.doi.org/10.1016/j.apcatb.2016.06.003.

References

[1] A.A. Mazioti, A.S. Stasinakis, G. Gatidou, N.S. Thomaidis, H.R. Andersen, Chemosphere 131 (2015) 117–123.
[2] J. Xu, L. Li, C. Guo, Y. Zhang, S. Wang, Chem. Eng. J. 221 (2013) 230–237.
[3] Y. Ding, C. Yang, L. Zhu, J. Zhang, J. Hazard. Mater. 175 (2010) 96–103.
[4] F.J. Benitez, J.L. Acero, F.J. Real, G. Roldan, E. Rodriguez, J. Hazard. Mater. 282 (2015) 224–232.
[5] Y. Jia, L. Molstad, Å. Frostegård, P. Aagaard, G.D. Breedveld, L.R. Bakken, Soil Biol. Biochem. 39 (2007) 1597–1608.
[6] P. Herrero, F. Borrull, E. Pocurull, R.M. Marcé, Trends Anal. Chem. 62 (2014) 46–55.
[7] S. Bahnmuller, C.H. Loi, K.L. Linge, U. Gunten, S. Canonica, Water Res. 74 (2015) 143–154.
[8] J. Wu, W. Pu, C. Yang, M. Zhang, J. Zhang, J. Environ. Sci. 25 (2013) 801–807.
[9] V.M. Monsalvo, J. Lopez, M. Munoz, Z.M. de Pedro, J.A. Casas, A.F. Mohedano, J.J. Rodriguez, Chem. Eng. J. 264 (2015) 856–862.
[10] Y. Huang, C. Cui, D. Zhang, L. Li, D. Pan, Chemosphere 119 (2015) 295–301.
[11] J. Xiao, Y. Xie, H. Cao, Chemosphere 121 (2015) 1–17.
[12] C. Wang, Y. Shih, Sep. Purif. Technol. 140 (2015) 6–12.
[13] C. Gong, J. Jiang, D. Li, Sci. Total Environ. 532 (2015) 495–500.
[14] T. Mackul'ak, A. Takáčová, M. Gál, M. Marton, J. Ryba, Polym. Degrad. Stab. 120 (2015) 226–231.
[15] C. Jiang, Z. Gao, H. Qu, J. Li, X. Wang, P. Li, H. Liu, J. Hazard. Mater. 250-251 (2013) 76–81.

[16] R. Huang, Z. Fang, X. Fang, E.P. Tsang, J. Colloid Interface Sci. 436 (2014) 258–266.
[17] A. Babuponnusami, K. Muthukumar, Sep. Purif. Technol. 98 (2012) 130–135.
[18] J. Song, H. Wang, G. Hu, S. Zhao, H. Hu, B. Jin, Mater. Res. Bull. 47 (2012) 3296–3300.
[19] G.M. ElShafei, F.Z. Yehia, O.I. Dimitry, A.M. Badawi, G. Eshaq, Ultrason. Sonochem. 21 (2014) 1358–1365.
[20] J. Zbiljic, O. Vajdle, V. Guzsvany, J. Molnar, J. Agbaba, B. Dalmacija, K. Kalcher, J. Hazard. Mater. 283 (2015) 292–301.
[21] Z. Wen, Y. Zhang, C. Dai, Z. Sun, J. Hazard. Mater. 287 (2015) 225–233.
[22] X. Hong, G. Zhang, Y. Zhu, H. Yang, Mater. Res. Bull. 38 (2003) 1695–1703.
[23] F. Qi, W. Chu, B. Xu, Chem. Eng. J. 262 (2015) 552–562.
[24] L. Zhang, Y. Nie, C. Hu, J. Qu, Appl. Catal. B 125 (2012) 418–424.
[25] H. Zou, S. Chen, Z. Liu, W. Lin, Powder Technol. 207 (2011) 238–244.
[26] K. Wang, Z. Shi, Y. Wang, Z. Ye, H. Xia, G. Liu, G. Qiao, J. Alloys Compd. 624 (2015) 85–93.
[27] M.T. Le, T.T. Nguyen, P.T.M. Pham, E. Bruneel, I. Van Driessche, Appl. Catal. A 480 (2014) 34–41.
[28] E. García-López, G. Marcì, F. Puleo, V. La Parola, L.F. Liotta, Appl. Catal. B 178 (2015) 218–225.
[29] J. Deng, L. Zhang, H. Dai, C.-T. Au, Appl. Catal. A 352 (2009) 43–49.
[30] T.-D. Pham, B.-K. Lee, C.-H. Lee, Appl. Catal. B 182 (2016) 172–183.
[31] L. Lyu, L. Zhang, C. Hu, Chem. Eng. J. 274 (2015) 298–306.
[32] X. Yao, Y. Xiong, J. Sun, F. Gao, Y. Deng, C. Tang, L. Dong, J. Rare Earths 32 (2014) 131–138.
[33] A.M. Abdelghany, H.A. ElBatal, J. Mol. Struct. 1067 (2014) 138–146.
[34] S. Rada, A. Dehelean, E. Culea, J. Alloys Compd. 509 (2011) 321–325.
[35] S.H. Kim, A. Umar, S.-W. Hwang, Ceram. Int. 41 (2015) 9468–9475.
[36] S. Ghasemi, R. Hosseinzadeh, M. Jafari, Int. J. Hydrogen Energy 40 (2015) 1037–1046.
[37] M. Bayat, M. Sohrabi, S.J. Royaee, J. Ind. Eng. Chem. 18 (2012) 957–962.
[38] S. Bahnmüller, C.H. Loi, K.L. Linge, U.v. Gunten, S. Canonica, Water Res. 74 (2015) 143–154.
[39] E.M. Matira, T.C. Chen, M.C. Lu, M.L. Dalida, J. Hazard. Mater. 300 (2015) 218–226.
[40] K. Choi, W. Lee, J. Hazard. Mater. 211-212 (2012) 146–153.
[41] E. Jover, V. Matamoros, J.M. Bayona, J. Chromatogr. 1216 (2009) 4013–4019.
[42] Y.-S. Liu, G.-G. Ying, A. Shareef, R.S. Kookana, Environ. Pollut. 165 (2012) 225–232.
[43] C.H. Loi, F. Busetti, K.L. Linge, C.A. Joll, J. Chromatogr. 1299 (2013) 48–57.
[44] T. Reemtsma, U. Miehe, U. Duennbier, M. Jekel, Water Res. 44 (2010) 596–604.
[45] L. Gu, N. Zhu, H. Guo, S. Huang, Z. Lou, H. Yuan, J. Hazard. Mater. 246-247 (2013) 145–153.
[46] Y. Ling, M. Long, P. Hu, Y. Chen, J. Huang, J. Hazard. Mater. 264 (2014) 195–202.
[47] L. Zhou, W. Song, Z. Chen, G. Yin, Environ. Sci. & Technol. 47 (2013) 3833–3839.
[48] L. Xu, J. Wang, Sep. Purif. Technol. 149 (2015) 255–264.
[49] M. Su, C. He, V.K. Sharma, M. Abou Asi, D. Xia, X.Z. Li, H. Deng, Y. Xiong, J. Hazard. Mater. 211–212 (2012) 95–103.
[50] W. Huang, M. Brigante, F. Wu, C. Mousty, K. Hanna, G. Mailhot, Environ. Sci. & Technol. 47 (2013) 1952–1959.
[51] M.-T. Nguyen-Le, B.-K. Lee, Chem. Eng. J. 281 (2015) 20–33.
[52] S.C. Smith, F. Ahmed, K.M. Gutierrez, D. Frigi Rodrigues, Chem. Eng. J. 240 (2014) 147–154.
[53] M. Finšgar, I. Milošev, Corros. Sci. 52 (2010) 2737–2749.
[54] H.C. Kim, M.J. Kim, T. Lim, K.J. Park, K.H. Kim, S. Choe, S.-K. Kim, J.J. Kim, Thin Solid Films 550 (2014) 421–427.
[55] Y. Miao, S. Wang, C. Wang, Y. Liu, M. Sun, Y. Chen, Microelectron. Eng. 130 (2014) 18–23.
[56] J. Wan, L. Zhou, H. Deng, F. Zhan, R. Zhang, J. Mol. Catal. A: Chem. 407 (2015) 67–74.
[57] W.-R. Chen, C.-H. Huang, Environ. Pollut. 159 (2011) 1092–1100.
[58] Z. Qu, R. Fan, Z. Wang, H. Wang, L. Miao, Appl. Surf. Sci. 351 (2015) 573–579.
[59] Y. Wang, Y. Xie, H. Sun, J. Xiao, H. Cao, S. Wang, J. Hazard. Mater. 301 (2015) 56–64.
[60] Z. Chen, L. Huang, G. Zhang, Y. Qiu, X. Guo, Corros. Sci. 65 (2012) 214–222.
[61] B. Xu, F. Wu, X. Zhao, H. Liao, J. Hazard. Mater. 184 (2010) 147–155.
[62] S. Saha, A. Pal, Sep. Purif. Technol. 134 (2014) 26–36.
[63] A. Fakhri, Ecotoxicol. Environ. Saf. 104 (2014) 386–392.
[64] P.F. Khan, V. Shanthi, R.K. Babu, S. Muralidharan, R.C. Barik, J. Environ. Chem. Eng. 3 (2015) 10–19.
[65] Y.H. Jo, S.H. Do, S.H. Kong, Chemosphere 95 (2014) 550–555.
[66] S.H. Do, B. Batchelor, H.K. Lee, S.H. Kong, Chemosphere 75 (2009) 8–12.